ARMY RESEARCH LABORATORY

Variable Rail Voltage Control of a Brushless DC (BLDC) Motor

by Yuan Chen, Joseph Conroy, and William Nothwang

ARL-TR-6308 **January 2013**

Approved for public release; distribution unlimited.

NOTICES

Disclaimers

The findings in this report are not to be construed as an official Department of the Army position unless so designated by other authorized documents.

Citation of manufacturer's or trade names does not constitute an official endorsement or approval of the use thereof.

Destroy this report when it is no longer needed. Do not return it to the originator.

Army Research Laboratory
Adelphi, MD 20783-1197

ARL-TR-6308 **January 2013**

Variable Rail Voltage Control of a Brushless DC (BLDC) Motor

Yuan Chen, Joseph Conroy, and William Nothwang
Sensors and Electron Devices Directorate, ARL

Approved for public release; distribution unlimited.

REPORT DOCUMENTATION PAGE

Form Approved
OMB No. 0704-0188

Public reporting burden for this collection of information is estimated to average 1 hour per response, including the time for reviewing instructions, searching existing data sources, gathering and maintaining the data needed, and completing and reviewing the collection information. Send comments regarding this burden estimate or any other aspect of this collection of information, including suggestions for reducing the burden, to Department of Defense, Washington Headquarters Services, Directorate for Information Operations and Reports (0704-0188), 1215 Jefferson Davis Highway, Suite 1204, Arlington, VA 22202-4302. Respondents should be aware that notwithstanding any other provision of law, no person shall be subject to any penalty for failing to comply with a collection of information if it does not display a currently valid OMB control number.
PLEASE DO NOT RETURN YOUR FORM TO THE ABOVE ADDRESS.

1. REPORT DATE *(DD-MM-YYYY)*
January 2013

2. REPORT TYPE

3. DATES COVERED (From - To)

4. TITLE AND SUBTITLE
Variable Rail Voltage Control of a Brushless DC (BLDC) Motor

5a. CONTRACT NUMBER

5b. GRANT NUMBER

5c. PROGRAM ELEMENT NUMBER

6. AUTHOR(S)
Yuan Chen, Joseph Conroy, and William Nothwang

5d. PROJECT NUMBER

5e. TASK NUMBER

5f. WORK UNIT NUMBER

7. PERFORMING ORGANIZATION NAME(S) AND ADDRESS(ES)
U.S. Army Research Laboratory
ATTN: RDRL-SER-L
2800 Powder Mill Road
Adelphi, MD 20783-1197

8. PERFORMING ORGANIZATION REPORT NUMBER
ARL-TR-6308

9. SPONSORING/MONITORING AGENCY NAME(S) AND ADDRESS(ES)

10. SPONSOR/MONITOR'S ACRONYM(S)

11. SPONSOR/MONITOR'S REPORT NUMBER(S)

12. DISTRIBUTION/AVAILABILITY STATEMENT
Approved for public release; distribution unlimited.

13. SUPPLEMENTARY NOTES

14. ABSTRACT

A brushless DC (BLDC) motor achieves higher energy efficiency and endures less wear and tear than a traditional brushed DC motor due to the lack of friction between current coils and motor brushes; it requires additional control logic, however, often implemented using a microcontroller, to perform motor commutation. Standard drive circuitry consists of a rail voltage applied to a three-phase inverter and a pulse width modulated (PWM) signal applied to MOSFET gates in accordance with the commutation pattern. Typically, motor speed control is achieved by varying the pulse width applied to the gates while maintaining a fixed rail voltage. We implemented a proportional-integral (PI) feedback system to control motor speed while varying rail voltage. Using this PI controller, we examined the relationship between steady-state power consumption and rail voltage for a fixed reference, as well as the effect of variable rail voltage on transient controller response and total transient power consumption.

15. SUBJECT TERMS
Variable speed control brushless DC motor

16. SECURITY CLASSIFICATION OF:			17. LIMITATION OF ABSTRACT	18. NUMBER OF PAGES	19a. NAME OF RESPONSIBLE PERSON
a. REPORT	b. ABSTRACT	c. THIS PAGE			William Nothwang
Unclassified	Unclassified	Unclassified	UU	30	19b. TELEPHONE NUMBER (*Include area code*) (301) 394-1163

Standard Form 298 (Rev. 8/98)
Prescribed by ANSI Std. Z39.18

Contents

List of Figures **iv**

Acknowledgments **v**

Student Biography **vi**

1. Introduction **1**

2. Background **1**

2.1 Sensorless BLDC Commutation 1

2.2 Proportional-integral Feedback Control 3

3. Implementation **5**

3.1 Proposed Modifications to Motor Drive 5

3.2 Controller Implementation 8

4. Experimental Setup **10**

5. Results and Discussion **12**

5.1 Steady State Power Consumption 12

5.2 Controller Response to Reference Step Inputs 15

6. Conclusions and Future Work **17**

7. References **18**

List of Symbols, Abbreviations, and Acronyms **19**

Distribution List **20**

List of Figures

Figure 1. A typical commutation scheme for BLDC motors with high side PWM where A+ represents the high side MOSFET of phase A and A- represents the low side MOSFET of phase A (*2*).....2

Figure 2. A typical BEMF pattern with zero crossings labeled (*7*). 3

Figure 3. Modified BLDC motor drive schematic.....7

Figure 4. Current sensor schematic.....10

Figure 5. Power consumption as a function of rail voltage for fixed motor speed.....12

Figure 6. Power consumption as a function of rail voltage in the 3.1 V to 3.5 V applied voltage range at reference speeds of (a-top left) 5000 rpm, (b-top right) 6150 rpm, (c-bottom left) 7300 rpm, and (d-bottom right) 8450 rpm. The error bars represent the standard deviation. 13

Figure 7. Controller response to step reference input from 5000 rpm to 7300 rpm at 5 V, 4 V, 3.2 V, and 3 V applied rail voltage. 15

Acknowledgments

I would like to acknowledge my mentors, Will Nothwang and Joe Conroy, for the tremendous amount of support and guidance they have given me over the course of this project. I am very grateful for both their technical contributions and their encouraging advice throughout the entire process. They have helped to make this an extremely fruitful and valuable experience.

Student Biography

Yuan Chen is a senior at Princeton University, working towards a bachelor's degree in electrical engineering, and pursuing certificate programs in robotics and intelligent systems, and the applications of computing. He is interested in the areas of signal processing and linear systems. Upon graduation, he hopes to attend graduate school, where he plans to focus on the field of signal processing.

1. Introduction

A brushless DC (BLDC) motor is a motor in which the electric coils are part of the stator, with permanent magnets placed on the rotor, whereas a standard (brushed) DC motor has the coils on the rotor, itself (*1*). The standard DC motor requires brushes to contact the rotor in order to transfer current into the coils. This contact introduces additional friction to the motor and causes wear and lower efficiency (*1*). The brushless motor does not require such contact, thereby avoiding the additional friction and improving overall motor efficiency. A BLDC, however, requires control system, often implemented using a microcontroller, to perform the motor commutation process.

A typical commutation system uses a three half-bridge circuit (three phase inverter) to drive current into individual BLDC coil phases (*2*). Typically, a pulse width modulation signal sent to gates of the inverter MOSFETs is used to control motor speed (*3*). By varying the duty cycle of the gate input signal, one controls the current input into the coils and, consequently, the motor speed. Whereas pulse width modulation (PWM) determines current by controlling gate voltage on the metal oxide semiconductor field effect transistors (MOSFETs) of the three-phase inverter, one can also determine current by changing the drain-source rail voltage. We can achieve open loop speed control to a fixed reference speed in a variable rail voltage environment.

2. Background

2.1 Sensorless BLDC Commutation

To physically turn the rotor, we apply current to two phases, while leaving the remaining phase floating. The process of current application to the motor requires exactly one of the high-side MOSFETs and one of the low-side MOSFETs to be in an “on” state. Moreover, the on-state MOSFETs from the top and bottom side of the driver must correspond to different motor phases, as turning on both transistors of the same phase creates a short from power to ground. Within a 360° electrical cycle, a phase follows a sequence of 120° high voltage, 60° floating, 120° low voltage, 60° floating. A typical scheme applies this electrical cycle to each of the three phases, with a 60° offset between each phase (*1*). We define commutation as the switching sequence of the three phases that causes the rotor to turn in the desired direction. In order to optimally commutate the BLDC motor, it is necessary to know the position of the rotor. A typical BLDC scheme for motor control is shown in figure 1. Whereas certain BLDC motors have built-in Hall Effect sensors for position detection, we consider a position detection scheme, which measures the back electromagnetic field (BEMF) signal from the floating phase.

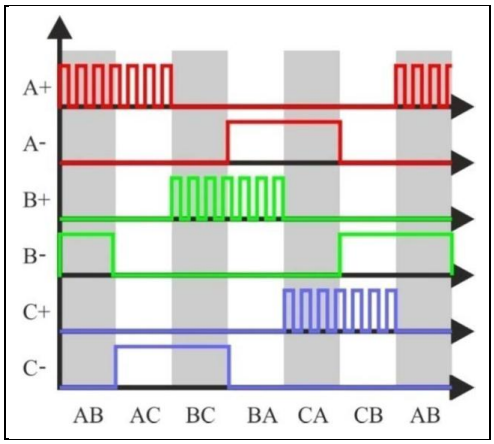

Figure 1. A typical commutation scheme for BLDC motors with high side PWM where A+ represents the high side MOSFET of phase A and A- represents the low side MOSFET of phase A (*2*).

For Y-configuration motors without access to a common/neutral point, BEMF is measured with respect to the applied rail voltage and ground. A typical BEMF pattern is shown in figure 2. The corresponding zero crossing of the signal occurs when the measured voltage is equal to one-half the applied voltage (*4*). In order to achieve optimal torque, the commutation should occur at a 30° phase delay from the zero crossing (*5*). Low pass filtering is required to remove the high frequency noise in the BEMF resulting from the motor drive PWM signal. At low PWM duty cycles, the magnitude of the BEMF signal is always less than the zero crossing voltage due to current flow through the body diode of low side MOSFETS during PWM off-time (*6*). In general, BEMF techniques are appropriate only for commutation above a limiting speed. Below this speed, the generated BEMF is too low in magnitude, and the measured signal has too low of a signal-to-noise ratio to consistently determine the position of the rotor, and for this reason, sensorless commutation techniques require an open-loop starting procedure (*5*).

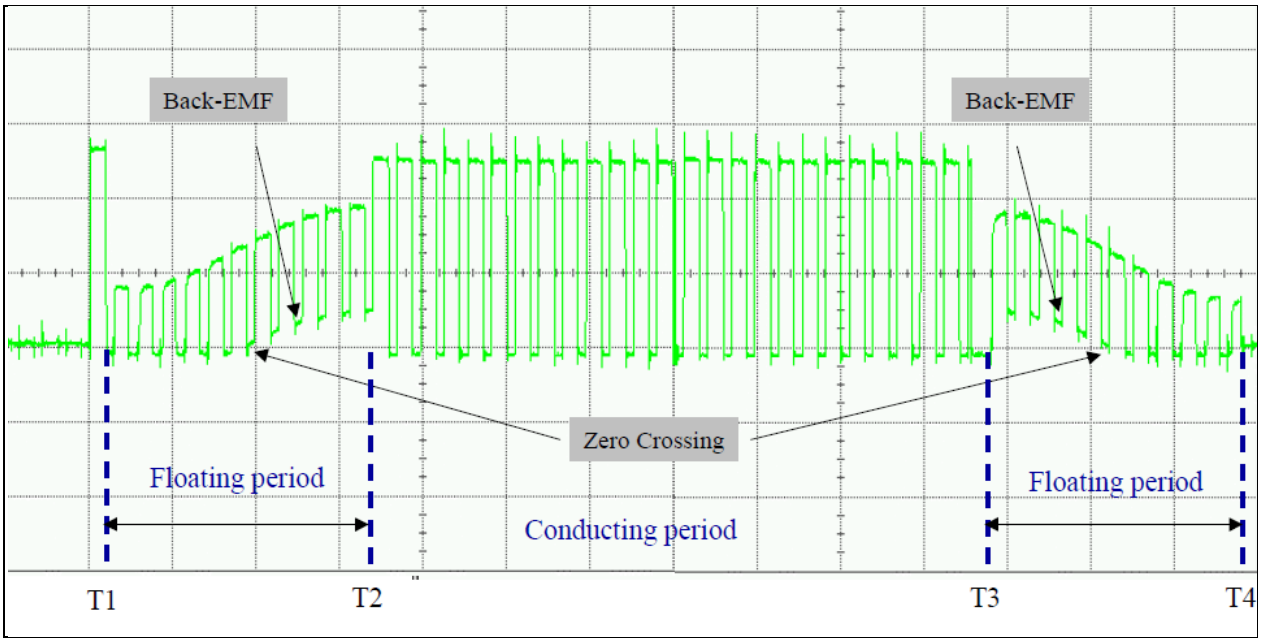

Figure 2. A typical BEMF pattern with zero crossings labeled (*7*).

Low pass filtering techniques introduce phase delay, which increases in magnitude with increasing frequency. Furthermore, filtering cannot completely eliminate the PWM noise without also attenuating the fundamental BEMF signal. An alternative to low pass filtering is to sample BEMF during PWM "on" time (*7*). Using the rising edge of the PWM signal to trigger BEMF sampling, we consider only BEMF values associated with PWM on time and ignore those values associated with PWM "off" time. This selective sampling technique removes the PWM noise from the BEMF signal and does not introduce phase delay in the output. The zero crossing point is calculated by directly comparing the sampled value against one-half the applied rail voltage.

2.2 Proportional-integral Feedback Control

Through modular treatment of the BLDC motor commutation logic, we model the motor behavior as a linear system. The system as a whole outputs angular velocity as a linear function of the input signal and performs commutation internally to meet this operation specification. In this case, the BLDC motor system has a transfer function of similar form to the standard brushed DC motor:

$$P(s) = \frac{K(v)}{\tau s+1}, \tag{1}$$

where v is the applied rail voltage. In typical fixed rail voltage applications, the motor plant has constant steady-state gain, and the constants K and τ can be determined through experimentation.

We achieve closed-loop feedback control using a proportional-integral controller, which has a transfer function of the form

$$C(s) = k_p + \frac{k_i}{s}. \tag{2}$$

The closed-loop system then has the transfer function

$$H(s) = \frac{P(s)C(s)}{1+P(s)C(s)}$$

$$= \frac{K(v)(sk_p+k_i)}{\tau s^2 + (1+K(v)k_p)s + K(v)k_i}. \tag{3}$$

For an input $x(t) = step(t)$, we compute the step response of the system as

$$y(t) = step(t) * h(t)$$

$$Y(s) = \frac{H(s)}{s}. \tag{4}$$

From the Final Value Theorem, we compute the steady state gain of the system:

$$\lim_{t\to\infty} y(t) = \lim_{s\to 0} sY(s). \tag{5}$$

$$\lim_{s\to 0} H(s) = 1, \tag{6}$$

where we reach the result in equation 6 by substituting in for the definition of $Y(s)$ into equation 5. With only the requirement that $K(v) \neq 0$ and no additional knowledge of $K(v)$, we achieve unitary gain and steady-state step reference tracking using the proportional-integral (PI) controller.

The closed-loop transfer function in equation 3 has a zero at $s = -\frac{k_i}{k_p}$, which is fixed by the controller gains. The poles of the system are determined by

$$s = \frac{-(1+K(v)k_p) \pm \sqrt{(1+K(v)k_p)^2 - 4\tau K(v)k_i}}{2\tau}. \tag{7}$$

By varying rail voltage, we also move the position of the system poles, and we expect a fixed gains controller to have time domain characteristics that vary with the applied rail voltage.

We derive a state-space form of the motor transfer function in equation 1 for the state $= \begin{bmatrix} \int_0^t \omega(\alpha)d\alpha \\ \omega(t) \end{bmatrix}$, which corresponds to the state feedback analog of the PI controller. For this choice of state vector, we obtain the state-space representation

$$\dot{\boldsymbol{x}} = \begin{bmatrix} 0 & 1 \\ 0 & -\frac{1}{\tau} \end{bmatrix} \boldsymbol{x} + \begin{bmatrix} 0 \\ \frac{K(v)}{\tau} \end{bmatrix} u, \tag{8}$$

$$y = [0 \quad 1]\boldsymbol{x}.$$

The state-space representation in equation 8 has the controllability matrix

$$\mathcal{C} = \begin{bmatrix} 0 & \frac{K(v)}{\tau} \\ \frac{K(v)}{\tau} & -\frac{K(v)}{\tau^2} \end{bmatrix}. \tag{9}$$

The determinant of $\mathcal{C}$ is given by $\det(\mathcal{C}) = -\frac{K(v)^2}{\tau^2}$, and from the controllability-rank theorem, the PI controller and its state feedback analog are controllable if and only if $K(v) \neq 0$. This is consistent with the result obtained earlier in the analysis of system steady-state gain.

We trivially assume that $K(0) = 0$ from the characteristic that the motor remains stationary when there is no applied rail voltage, regardless of the reference speed input. We further assume that there exists a rail voltage level, v_0, such that $|K(v)| > 0, \forall v > v_0$. From the results in equations 6 and 9, we see that all system states are reachable and the controller tracks references with zero steady state error if we ensure that rail voltage is greater than v_0. This result does not always hold in practice, since the system transfer function in equation 1 is only valid for the sensorless feedback operation stage BLDC commutation. This operation requires that the motor run at a minimum non-zero angular velocity so that the BEMF signal has adequate amplitude for zero-crossing detection.

3. Implementation

3.1 Proposed Modifications to Motor Drive

We modified the standard design of the three-phase inverter BLDC motor drive to better accommodate the varying rail voltage. The standard three-phase inverter consists of three half–bridges, with the source of the high side P channel MOSFETs connected to the positive rail voltage. An enhancement mode P channel MOSFET conducts current if and only if $-V_{gs} > -V_t$, where V_{gs} is the gate-source voltage and V_t is the MOSFET threshold voltage, which is a physical characteristic of the individual component. The digital output of a microcontroller supplies the signal to the gate, and this digital output cannot take on a continuous range of values. The logical low state of the output corresponds to the conducting state of a P channel enhancement MOSFET, and similarly the logical high state corresponds to the non-conducting state.

In the logical low state of the digital output gate signal, $-V_{gs} = V_s$, where V_s is the applied rail voltage. To ensure that the high side MOSFET conducts as desired, we must select a component in which $-V_t$ is less than the minimum rail voltage. In the logical high state of the gate signal $-V_{gs}$ also varies with the applied rail voltage. If we do not modify the gate signal, then there is the additional constraint that $-V_{gs} < -V_t$ when the output is in logical high for the entire range of rail voltages so that the high side MOSFET shuts off as desired. An alternative to finding a component which meets both of these constraints is to perform a level shift of the gate

signal to the rail voltage. The logical high state of the shifted signal guarantees that $V_{gs} = 0$, and the high side MOSFET does not conduct during high output.

We use a tri-state buffer and line driver (CD74HC541) to perform the level shift. The component drives enough current to the MOSFET gate so that the gate signal rise time is negligible relative to the PWM frequency. The modified drive circuit delivers the gate signal without distortion associated with rise time to the high side P channel MOSFET (IRF4905) for the PWM frequency of 25 kHz. The tri-state buffer component creates more noise in the overall drive system, making it necessary to incorporate low pass filtering components to attenuate the additional noise. Specifically, the component creates additional noise on the power rails during motor operation, which in turn causes N channel MOSFET (IRF3703) behavior deviating from ideal operation. During the associated commutation on time for the low side MOSFET, the noise in the power supply causes undesired shutoff.

To perform sensorless BLDC commutation, it is necessary to generate undistorted BEMF signals. The undesired shutoff of the low side MOSFETs results in a higher amplitude PWM noise component. The commutation logic we implement applies a PWM signal to the high side gate and a binary (100% duty cycle) signal to the low side gate. In this implementation, the ideal BEMF during phase-high time contains PWM noise, associated with the individual on/off sequence of the high side gate, and the ideal BEMF during phase-low time does not contain PWM noise and remains at 0 V for the duration of phase-low time. Because the PWM noise exists in the phase-high time, PWM noise also exists in the signal during phase floating time. The added noise from the tri-state buffer and associated low side MOSFET shutoff causes the BEMF signal during phase low time to also contain PWM noise. This corruption of the BEMF signal disrupts calculation of the zero crossing point necessary for proper commutation timing.

To mitigate the corruption, we add a resistor in series between the output of the tri-state buffer and the gate of the low side MOSFET. The additional resistance acts as a low pass filter on the signal to the gate, and attenuates the PWM noise and voltage spikes associated with motor operation. The resulting BEMF signal of the drive circuit with gate signal low pass filtering behaves ideally during phase-low time, maintaining a constant 0 V level. The inclusion of the resistor in the drive circuitry introduces a second form of distortion in the BEMF signal. During the phase-high and floating phase portions of the commutation sequence, the signal consists of an impulse-duration peak to the appropriate voltage level (i.e., rail voltage level during PWM on-time) but decays quickly to approximately one-half the maximum amplitude reached. This form of distortion also disrupts calculation of the zero crossing point.

Specifically, the peak and decay characteristic of BEMF adversely affect the PWM rising-edge-triggered sampling technique used to remove PWM noise. Because the peak in the BEMF signal occurs almost instantaneously, a microcontroller does not have adequate time to perform sampling and comparison. Using a programmable embedded system on a chip (PSoC)-5 (Cypress Semiconductor) microcontroller's comparator component triggered on the rising edge

of the PWM output, we cannot consistently perform the BEMF sampling. The comparator output alternates between logical high and logical low during phase on time, whereas the ideal comparator output remains logical high for the entire duration of phase on time. By adding capacitance to ground in the BEMF circuit, we implement a low pass filtering of the signal. The additional capacitance prevents the quick decay of BEMF but also increases signal rise time. As a result, BEMF does not instantaneously rise to its maximum value, and it is no longer appropriate to sample on the PWM rising edge. Instead, we can accurately detect the zero crossing point by sampling BEMF at one-half of the on time.

The schematic of the proposed drive system is shown in figure 3, which shows the specific values of the low side gate resistor and BEMF ground capacitor. The MOSFETs selected for the drive system (IRF4905, IRF3703) have threshold voltages of -4.0 V and 4.0 V, respectively. In order to achieve a wider rail voltage range, it is necessary to replace these components with MOSFETs with lower magnitude threshold voltage.

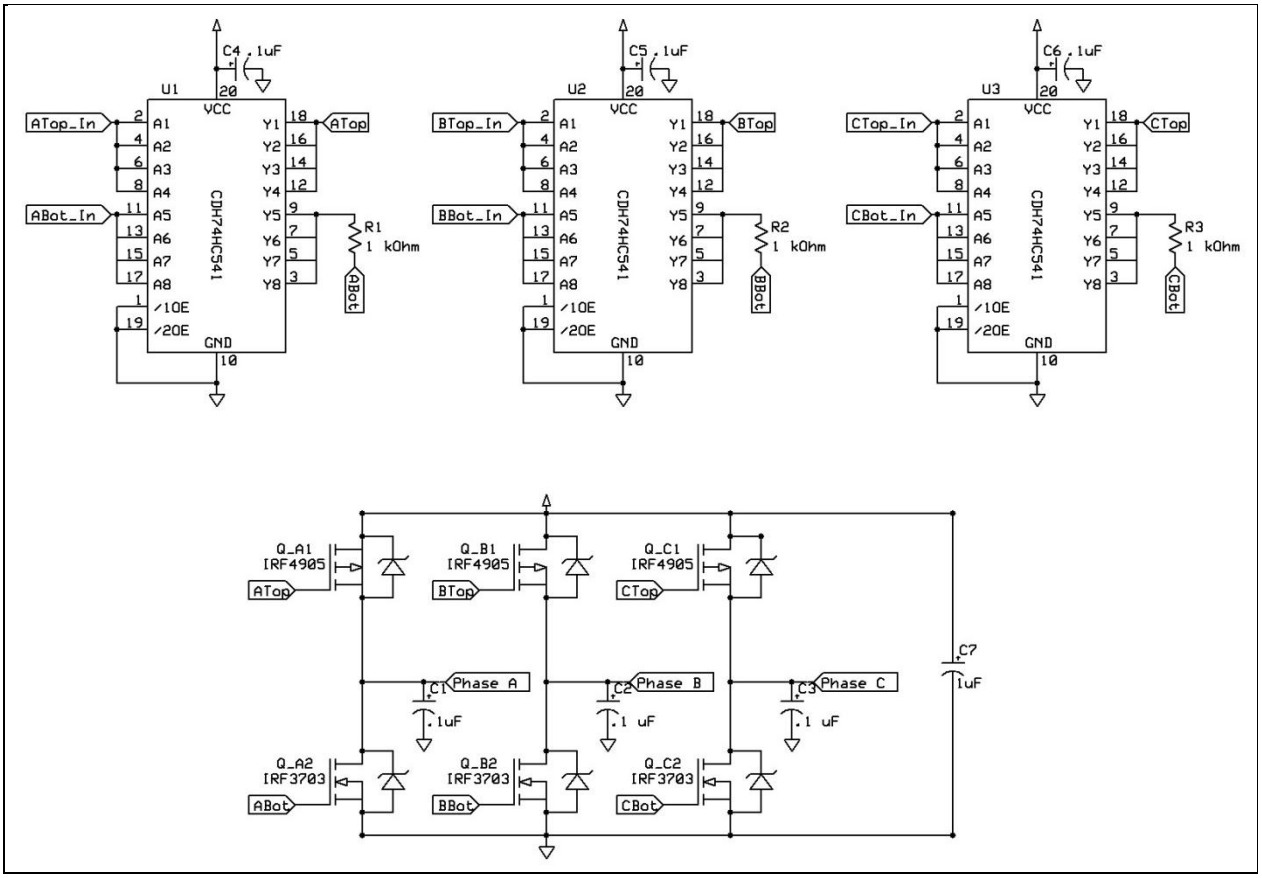

Figure 3. Modified BLDC motor drive schematic.

We attempt to implement sensorless commutation using the PSoC-5 microcontroller and the modified hardware drive circuitry. Although we verify the implementation of the commutation sequence logic and successfully achieved free running commutation, we cannot consistently

transition to sensorless commutation; that is, while we can artificially time and force the commutation progression, we cannot detect the proper commutation timing from BEMF sensing. Additional work is required on the proposed modified BLDC motor drive and sensorless commutation mechanism in noise reduction and BEMF sensing before it can be used in practical applications.

3.2 Controller Implementation

To ensure consistent operation, we use an existing hardware setup to perform motor commutation. The existing hardware uses an 8-bit Atmel microcontroller, which requires a 5 V power source, to implement the sequential commutation logic. The board housing the Atmel microcontroller also contains inputs for a separate motor power source and pins providing access to the commutation signals. The microcontroller accepts as input a pulse with width between 1 ms and 2 ms, where a 1 ms pulse corresponds to the motor-off state, and a 2 ms pulse drives the motor at the maximum angular velocity. This existing hardware acts as an open loop speed controller for the BLDC motor as output motor speed changes for varying load and fixed input pulse width.

We implement a feedback controller using the PSoC-5 microcontroller, which sends the necessary pulse width signal to drive the Atmel controller and estimates speed based on the commutation signal output. We choose to observe the commutation signal of a single high side gate since the Atmel controller applies only a binary level signal to the high side MOSFETs. We measure T, the commutation period, as the time between two rising edges of the high side commutation signal. From the measurement of T in seconds, we calculate the motor angular velocity in rotations per minute as

$$\omega = \frac{60}{NT}, \tag{10}$$

where N is the number of magnet pairs in the motor. We use a BLDC motor with $N = 5$.

On each rising edge of the commutation signal, the feedback controller computes the observed angular velocity and the error $e(t)$ from the reference input $r(t)$

$$e(t_m) = r(t_m) - \omega(t_m), \tag{11}$$

where time t is indexed in m to indicate that the controller reads a discrete sampling of time instead of a continuous time spectrum. Furthermore, because we use a discrete time scale, we cannot directly calculate the integral of the error and, instead, approximate the term as a summation

$$\int_0^{n_0} e(\alpha)d\alpha \approx \sum_{m=0}^{M} e(t_m)T_m, \tag{12}$$

where $t_M = n_0$ and $\sum_{m=0}^{M} T_m = n_0$. For consistency in scaling, we express all angular velocity terms in units of revolutions per minute and all time terms in units of seconds.

With each update of the error term and error integral term, the PSoC-5 outputs a pulse to the Atmel controller to adjust the open loop speed setting. The feedback system calculates the raw pulse width $x(t_M)$ in units of 10 μs, and the function has the form

$$x(t_M) = x_0 + k_p e(t_M) + k_i \sum_{m=0}^{M} e(t_m) T_m. \tag{13}$$

The offset term x_0 improves controller resolution by biasing its output range, and we choose $x_0 = 99$, which corresponds to the minimum valid input pulse width of 1 ms. We refer to $x(t_m)$ as a raw pulse width since we do not constrain the result to be within the valid pulse width input range of the Atmel controller. The true output $u(t_M)$ of the PSoC-5 controller has pulse width determined by

$$u(t_M) = \begin{cases} x_l, & x(t_M) < x_l \\ x(t_M), & x_l \leq x(t_M) \leq x_h \\ x_h, & x(t_M) > x_h \end{cases}. \tag{14}$$

We experimentally find $x_l = 107$, corresponding to a pulse width of 1.08 ms, as an appropriate setting of the lower bound. Below this pulse width, the Atmel controller does not consistently operate the BLDC motor at 5 V rail voltage and non-zero load, since sensorless commutation requires a minimum angular velocity to generate adequate amplitude BEMF. We further experimentally find that $x_h = 159$, corresponding to a pulse width of 1.60 ms, as an appropriate setting of the upper bound. Above this pulse width, we observe physical instability in our motor setup. Due to these bounds on the range of pulse width output, we constrain the reference speed inputs to be between 4500 rotations per minute (rpm) and 10,000 rpm. We choose controller gains of $k_p = 0.1$ and $k_i = .025$. Recall that equation 3 states the controller has a transfer function of the form $C(s) = k_p + \frac{k_i}{s}$.

We also implement the capability to adjust the reference speed externally. The PSoC-5 controller takes as input a pulse between 1 ms and 2 ms, and sets the reference speed to a value in the defined range. We use a counter component to measure the width of the pulse. We connect the counter's enable pin to the input pulse so that it only operates during the signal's logic high level. The counter outputs a capture value, equivalent to the elapsed time in microseconds, on the falling edge of the input signal and resets following the capture procedure. The PSoC-5 controller then sets the reference speed as a function of the capture value γ

$$r = 5\gamma - 750. \tag{15}$$

We choose the constants, which define the mapping from γ to r, such that a pulse width of 1050 μs corresponds to a reference speed of 4500 rpm, and a pulse of 1950 μs corresponds to a reference speed of 9000 rpm. These two points define a function that we extrapolate over the defined interval of reference speeds from 4500 rpm to 10000 rpm. We also implement a special case for setting a zero reference speed when the input pulse has a pulse width between 1.00 ms and 1.04 ms.

4. Experimental Setup

We design and conduct experiments to measure the power consumption for fixed motor speed as a function of applied rail voltage and the transient response of the speed controller as a function of the applied rail voltage. These experiments require measurement of the rail voltage, current consumption of the motor drive circuit, and motor speed. While rail voltage can be measured directly, current and motor speed require additional conversion and sensing circuitry. We implement a current-to-voltage convertor using a shunt resistor and difference amplifier, since it is easier to measure voltage than current. Direct measurement of motor speed requires additional electronics, such as Hall Effect or optoelectronic sensors. Alternatively, we use the commutation signals in the same fashion as the feedback controller to measure motor speed in these experiments. We make all measurements using a LabView-based data acquisition system.

The current-to-voltage convertor consists of a high side shunt resistor R_s and a difference amplifier. We show the schematic for the current sensor in figure 4.

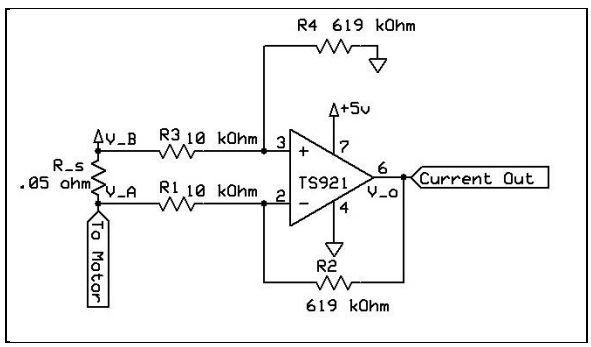

Figure 4. Current sensor schematic.

The TS921 operation amplifier is a single supply rail-to-rail component and is powered by a +5 V source separate from the motor drive power source. This +5 V supply is the same supply that powers all other components separate from the motor drive, including the Atmel microprocessor. The overall system requires an operational amplifier with single supply operation mode since there is no –5 V supply available. The lack of negative voltage requires rail-to-rail operation mode to enable accurate sensing of low current levels.

The difference amplifier in figure 4 has a transfer function of the form

$$V_o = \frac{V_B R_4 (R_1 + R_2)}{R_1 (R_3 + R_4)} - \frac{V_A R_2}{R_1}, \tag{16}$$

where V_o is the output voltage, V_B is the high side voltage (connected through R_3 to the non-inverting input), and V_A is the low side voltage (connected through R_1 to the inverting input). In the case that $R_1 = R_3$ and $R_2 = R_4$, equation 16 reduces to

$$V_o = \frac{R_2}{R_1}(V_B - V_A). \tag{17}$$

From equation 17, we derive a relation between the output voltage V_o and the motor drive current I

$$I = \frac{V_o R_1}{R_2 R_s}, \tag{18}$$

where we use the relation $V_B - V_A = IR_s$, a result from Ohm's Law. R_s is a sensing shunt resistor of low resistance so that there is minimal voltage drop. The gain of the amplifier $\frac{R_2}{R_1}$ is high enough such that low current can be sensed with fidelity against noise, and low enough such that high current does not cause amplifier saturation. We select precision ($\pm 1\%$ accuracy) resistors: $R_s = 0.05\ \Omega$, $R_1 = 10\ k\Omega$, and $R_2 = 619\ k\Omega$.

To compute power consumption, we measure the motor drive current and applied rail voltage for fixed reference speed. The data collection system samples each of the desired measurements at a rate of 10,000 Hz and outputs the average of every 2000 samples as a data point; the effective data output rate is 5 Hz. The averaging procedure is necessary to attenuate the noise in measurements. For a fixed reference speed, we vary applied rail voltage from 5.0 V to 3.0 V in increments of 0.2 V. It is still necessary to measure the real rail voltage applied to the motor drive because we use a high side current sensor. The voltage drop across the sensing resistor varies with applied voltage and causes a deviation of the measured voltage from the applied voltage. Additionally, variations in current for fixed applied voltage also cause variations in the measured rail voltage.

For each applied rail voltage level, we take the average of 50 data points (equivalent to 100,000 raw data points) for each measurement. That is, we consider the average of measured rail voltage to be the measured rail voltage for all data points of the same applied rail voltage. We also average the current for corresponding data points. The additional averaging further attenuates the noise in the current, as well, leading to a more reliable measurement of power consumption. The power consumption is associated with an applied rail voltage level to the product of the average measured rail voltage and the average measured motor drive current. We repeat this procedure for the reference speeds of 5000 rpm, 6150 rpm, 7300 rpm, and 8450 rpm, generating power consumption curve as a function of applied rail voltage for each of the references.

Additionally, we measure the transient response of the controller to a step input. Whereas the controller step response is typically measured with a step input reference from 0 to a fixed constant value, we use a step reference from 5000 rpm to 7300 rpm. This is to ensure that the motor operates in sensorless commutation mode during the duration of the experiment, and the step response is representative of the controller and not the BLDC starting procedure. We repeat the procedure using a fixed step reference at applied rail voltage levels of 5.0 V, 4.0 V, 3.2 V, and 3.0 V. The data collection system samples the output speed at a rate of 10000 Hz and outputs the average and standard deviation of every 50 samples as a data point; the effective data output

rate is 200 Hz. The results of this experiment are more susceptible to noise than the measurements of power consumption due to a smaller averaging window. The higher effective output rate is, however, required to capture the transient controller response with more appropriate time resolution. Due to susceptibility to noise, we examine the results of the controller step response measurements only for qualitative observations.

5. Results and Discussion

5.1 Steady State Power Consumption

From measurements of rail voltage and motor drive current, we compute the motor power consumption as a function of rail voltage for fixed motor speed and report the results in figure 5.

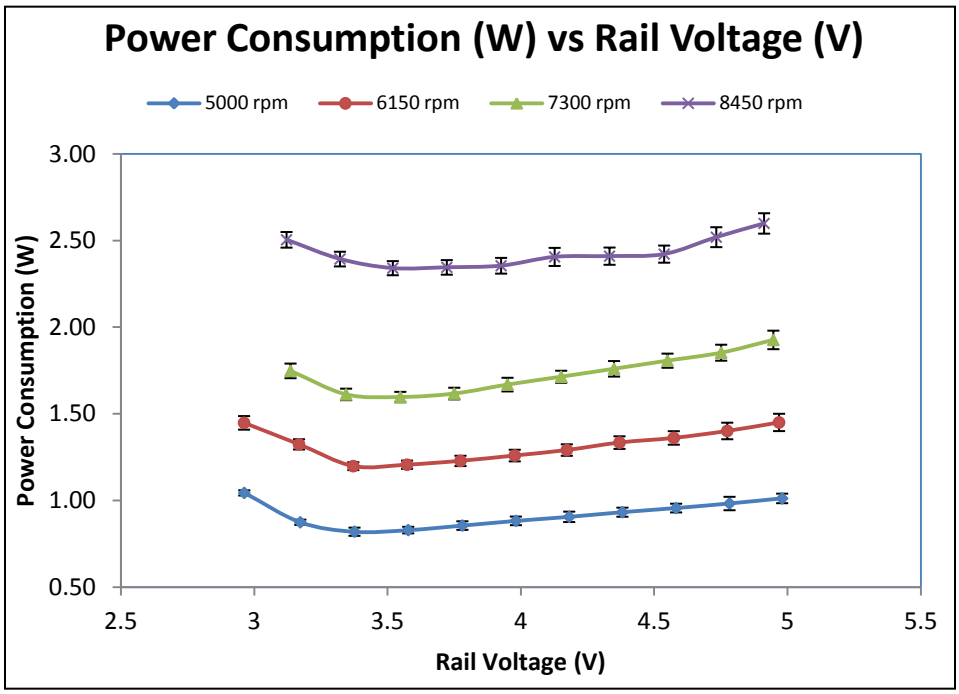

Figure 5. Power consumption as a function of rail voltage for fixed motor speed.

Figure 5 does not contain data points for the 3.0 V applied rail voltage at 7300 rpm and 8450 rpm because the controller does not track these reference speeds at the specified rail voltage. The higher current demand of these higher reference speeds causes a greater voltage drop across the shunt resistor and raises the lower bound of possible applied voltage. In addition, the physical properties of MOSFETs used in the drive circuitry may impose a limitation on the total current at low rail voltage. Consequently, the range of reachable motor speeds decreases for low applied rail voltage. This is a deviation from the theoretical result of controllability computed using the

state-space representation of equation 9. Under conditions of low rail voltage, the transfer function of equation 1 is no longer an appropriate model for the BLDC motor.

From figure 5, we note that for the chosen reference speeds, there exists a local minimum of power consumption in the voltage range of interest. The power consumption versus rail voltage curves have similar characteristics across the examined reference speeds. Increasing the rail voltage from 3.0 V (or the minimum voltage required for accurate tracking in the cases of 7300 rpm and 8450 rpm), power consumption decreases until it reaches local minimum in the 3.0 V to 4.0 V range. We also observe that the value of the local minimum varies with reference speed, and we note that this value increases with increasing reference speed. These are qualitative observations, since we only conducted the steady state power consumption for four reference speeds. In order to determine a more reliable quantitative relationship between minimum power consumption and reference speed, it is necessary to conduct a similar experiment with a greater number of reference speeds to give the resulting relation more resolution in the independent variable.

We repeated the power consumption versus rail voltage experiment at an applied voltage range of 3.1 V to 3.5 V to capture the decreasing power consumption characteristic in greater detail. We report the results in figure 6.

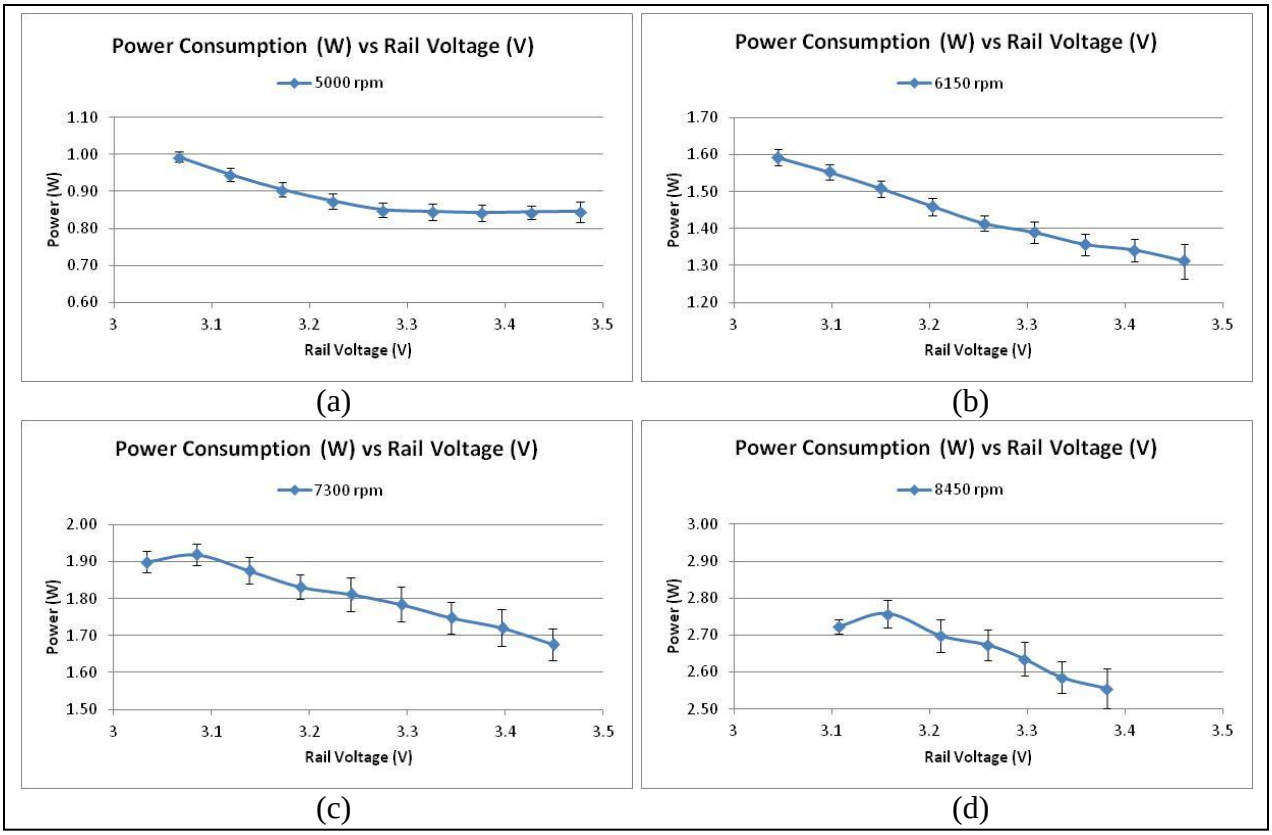

Figure 6. Power consumption as a function of rail voltage in the 3.1 V to 3.5 V applied voltage range at reference speeds of (a-top left) 5000 rpm, (b-top right) 6150 rpm, (c-bottom left) 7300 rpm, and (d-bottom right) 8450 rpm. The error bars represent the standard deviation.

Similar to the high voltage range experiment, there is a difference between the applied rail voltage and the measured rail voltage due to the voltage drop over the current sensing shunt resistor. In general, there is a larger voltage drop at higher reference speeds due to the larger required current. We also omit the two lowest applied rail voltage data points for the 8450 rpm reference since the controller does not track the reference accurately at these applied rail voltage levels. We do not omit any data points for the remainder of the reference speeds for the 3.1 V to 3.5 V applied voltage range.

Figure 6a shows that power consumption decreases from 3.07 V to 3.27 V of measured rail voltage and remains nearly constant for the remainder of the applied voltage range for a 5000 rpm reference speed. From figure 5, we know that power consumption increases as we increase the rail voltage above this range, and we conclude that the local minimum of power consumption for the 5000 rpm reference occurs in the measured rail voltage range of 3.27 V to 3.5 V. Conversely, figures 6b, c, and d show that power consumption continues to decrease at the highest measured rail voltage in this specified voltage range for higher reference speeds. We infer that the local minimum occurs at a rail voltage higher than 3.5 V, and using additional information in figure 3, we can qualitatively approximate that the rail voltage of minimum power consumption increases with increasing reference speed input.

An additional feature present in the results of the low voltage range experiment and absent from the high voltage range experiment is the apparent local maxima in power consumption for the 7300 rpm and 8450 rpm references. For both reference speeds, the steady state power consumption first increases with increasing rail voltage from the minimum capable voltage required for accurate tracking. We do not observe this feature in figure 3 since the high range of rail voltage and choice of increment between applied voltage levels does not provide adequate resolution. Recall that the lower bound of applied rail voltage in this experiment roughly defines the minimum rail voltage required to track the desired range of reference motor speeds, and the controller can track lower reference speeds at applied rail voltage levels lower than this bound. Therefore, it is also possible that local maxima also exist for lower reference speeds at a rail voltages lower than the range of applied rail voltages for this experiment.

The results of this experiment only give the relation between power consumption and rail voltage in the steady state. At the experiment's effective data output rate of 5 Hz, there are a negligible number of data points that represent the transient state between different levels of applied rail voltage due to the fast controller response. The data collection system does not measure with adequate resolution the transient power consumption of the controller's response to disturbances in rail voltage, and, thus, this experiment does not quantify the power consumed to change the operating rail voltage. In order to capture transient power consumption due to shifts in voltage, it is necessary to output data at a faster rate, which using our current experimental setup, results in high noise content in the output.

5.2 Controller Response to Reference Step Inputs

We examine the controller response to a step input in the reference speed and report the results in the figure 7.

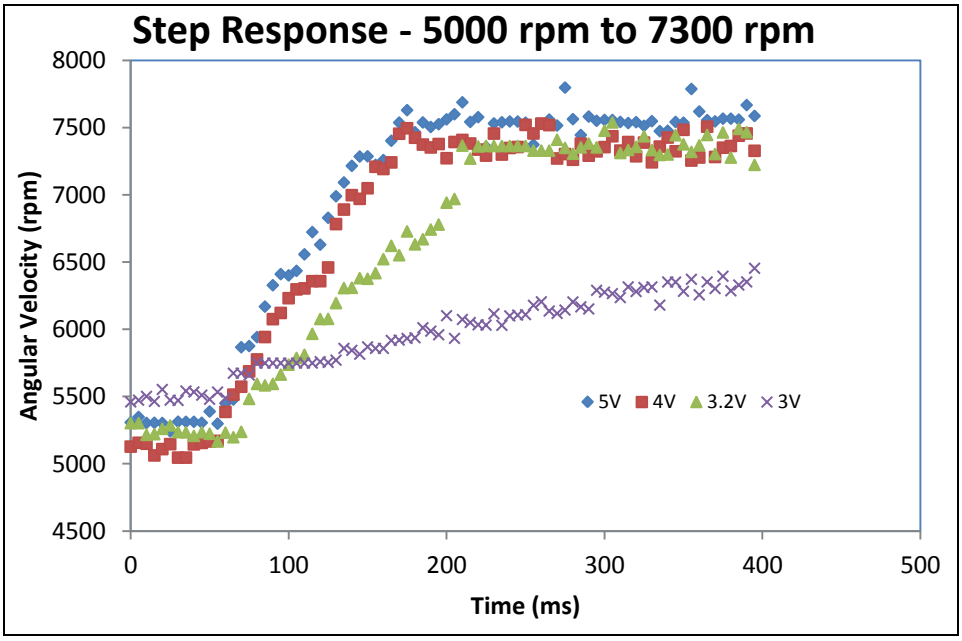

Figure 7. Controller response to step reference input from 5000 rpm to 7300 rpm at 5 V, 4 V, 3.2 V, and 3 V applied rail voltage.

In each of the plotted step responses, the shift in reference speed occurs at time 0 ms; that is, we plot the response immediately following step input to 400 ms after the reference shift. Each plotted response corresponds to a single step input (not the average of multiple inputs). The results of this experiment are, thus, more affected by noise in the measurements and are meant to give only a qualitative description of controller response. Recall, also, that we increase the effective output rate in order to capture transient response with adequate resolution, and this, too, increases the amplitude of noise in the data. We cannot reliably assign time domain specifications such as rise time, overshoot, and settling time to controller response in relation to the applied rail voltage. Rather, the results of this experiment give a qualitative description of the changes in controller step response with varying rail voltage.

The nominal values of 5 V, 4 V, 3.2 V, and 3 V represent the applied rail voltage from the power source. The voltage drop across the current sensing shunt resistor increases with decreasing applied rail voltage because of the larger current required to maintain reference tracking. This also implies a change in the measured rail voltage with the step input, since the higher reference input requires a larger current. This discrepancy between the measured rail voltage at the low and high reference speed levels differs with the applied rail voltage, as the difference in current required for tracking the individual speeds varies with applied rail voltage. We do not

automatically adjust for this change in measured rail voltage and report the controller response only in association with a nominal applied voltage level.

We observe a delay on the order of magnitude of 50 ms in controller response near the beginning of the step input. During this delay, the controller maintains tracking of the low reference speed, and the output speed begins rising only after this delay period. This pure delay is the delay from when the reference change is commanded to when the reference change is actually implemented. This delay is due to the experimental setup and will not impact the final design.

From figure 7, we see that the controller has similar step input rise time for 5 V and 4 V applied rail voltage settings, but the rise time is noticeably longer for the 3.2 V input. The rise time is significantly longer for the 3 V input, and the system does not track the higher reference speed. This is consistent with results from the steady state power consumption experiment, as the controller does not track a 7300 rpm reference input at 3 V for either setup.

We observe noise and oscillation in the controller response for 5 V, 4 V, and 3.2 V applied rail voltage levels. This oscillation, however, does not result from inadequate damping and low phase margin, but rather from error in measuring the input reference signal and the output speed. The step responses do not show any overshoot in output speed, implying that the current values of k_p and k_i produce an over-damped closed loop system for the 3.2 V to 5 V rail voltage interval. The step response of an over-damped system does not contain oscillations since the system poles are purely real. The sources of noise in the output are the speed sensing process internal to the controller, the reference speed input process, and the speed measuring process of the external data collection system. Each of these processes relies on the precise timing of a pulse width or frequency with resolution on the order of magnitude of 1 μs. A disturbance of 1 μs in the reference speed input causes a 5 rpm error from the desired reference. Further sensor noise in measuring motor speed causes noise in the output of the feedback controller.

Since the chosen values of k_p and k_i produce an over-damped system, increasing the value of k_i can improve controller rise time without being significantly detrimental to the overshoot and settling time. The over-damped system also has a large phase margin against instability, and it is possible to trade off this large phase margin for quicker response. Because rise time increases with decreasing rail voltage and the system is over-damped, the mean of the poles must decrease in magnitude with decreasing rail voltage. From equation 7, the mean of the poles is determined by $\sigma = -\frac{1+K(v)k_p}{2\tau}$, and from this result, $K(v)$ is decreasing with decreasing v. This is consistent with the intuition that the motor has smaller magnitude open loop gain with smaller applied rail voltage. The exact effect of a variable $K(v)$ on the closed loop system response depends on the exact values of k_p and k_i, and the general categorization of the system as over-damped, under-damped or critically damped.

From the results of the power consumption experiments, we conclude that a local minimum in power consumption exists in a rough range between 3.0 V and 4.0 V, depending on the motor

rpm. On this interval of rail voltage, we observe a qualitative increase in rise time with decreasing rail voltage. The combined results of the power consumption experiment and the step response experiment indicate that a tradeoff exists between steady state power consumption and fast controller response. There was minimal noted improvement in response time between 4 V and 5 V operation; though, power increased by 10–20% depending on RPM by changing the rail voltage from 4 V to 5 V. Operating at a lower rail voltage on this interval sacrifices response time to consume less steady state power, but operating at a higher rail voltage consumes more power yet improves controller response.

6. Conclusions and Future Work

We show that for our combination of motor, controller, and hardware drive circuitry, a local minimum in power consumption exists in the chosen rail voltage interval of 3 V to 5 V. For the reference speeds of 5000 rpm to 8450 rpm, this local minimum occurs specifically in the voltage interval between 3.2 V and 4.0 V. The value of the minimum power consumption operating voltage increases with increasing reference speed. Because the model of the BLDC motor plant changes with rail voltage, the controller time domain characteristics also change with rail voltage. We choose our feedback gains so that the overall system is over-damped in the chosen rail voltage interval, and observe that the system rise time increases with decreasing rail voltage. This suggests that a tradeoff exists between low steady state power consumption and fast transient system response. Although the results of our experiments pertain only to the specific combination of motor, controller, and hardware, we can apply the procedure of determining the relationship between power consumption and rail voltage to any such combination. That is, we can repeat the power consumption experiment with any set of motor, controller, and hardware drive circuitry.

An immediate future goal of this work is to implement both the feedback speed controller and commutation controller using an ARM microcontroller (Texas Instruments). We seek to ultimately implement this system as a component of a small, autonomous quad rotor robot. Other longer term goals include developing and implementing an optimal controller to autonomously select the desired operating rail voltage, and implementing a variable gain feedback controller to compensate for controller response characteristics in a variable rail voltage environment. Through the use of a digital potentiometer, one can implement a microcontroller determined variable voltage source. Given current measurements, the microcontroller internally calculates steady state power consumption, and through optimization techniques such as gradient descent, can autonomously determine an operating point of minimum power consumption. A further improvement to an autonomous variable rail voltage is to implement an optimal controller using linear quadratic regulation to choose operation points based on relative weight of power consumption and controller response.

7. References

1. Wilberg, J. Control of a Brushless DC Motor in a Shift by Wire System. M.S. Thesis, Linköpings University, Sweden, 2003.
2. Gamazo-Real, J. C.; Vázquez-Sánchez, E.; Gómez-Gil, J. Position and Speed Control of Brushless DC Motors Using Sensorless Techniques and Application Trends. *Sensors* [Online] **2010**, *10*, 6901–6947.
3. Muir, P.; Neuman, C. P. Pulsewidth Modulation Control of Brushless DC Motors for Robotic Applications. *IEEE Transactions on Industrial Electronics* [Online], **1985**, *IE-32-3*, 222–229.
4. Brown, W. Brushless DC Motor Control [Online]; Microchip Technology Inc.: Chandler, AZ, 2002; AN857.
5. Acarnley, P. P.; Watson, J. F. Review of Position-Sensorless Operation of Brushless Permanent-Magnet Machines. *IEEE Transactions on Industrail Electronics* [Online], **2006**, *53-2*, 352–362.
6. Shao, J. Direct Back EMF Detection Method for Sensorless Brushless DC (BLDC) Motor Drives. M.S. Thesis. Virginia Polytechnic University, Blacksburg, VA, 2003.
7. Gu, D.; Huang, J. Sensorless BLDC Motor control based on CY8C3866AXI [Online]; Cypress Inc.: San Jose, CA, 2009; AN58261.

List of Symbols, Abbreviations, and Acronyms

BEMF	back electromagnetic field
BLDC	brushless direct current (motor)
MOSFETs	metal oxide semiconductor field effect transistors
PI	proportional-integral (controller)
PSoC	programmable embedded system on a chip
PWM	pulse width modulation
RPM	rotations per minute

NO. OF COPIES	ORAGANIZATION
1 (PDF only)	DEFENSE TECHNICAL INFORMATION CTR DTIC OCA 8725 JOHN J KINGMAN RD STE 0944 FORT BELVOIR VA 22060-6218
1	DIRECTOR US ARMY RESEARCH LAB IMAL HRA 2800 POWDER MILL RD ADELPHI MD 20783-1197
1	DIRECTOR US ARMY RESEARCH LAB RDRL CIO LL 2800 POWDER MILL RD ADELPHI MD 20783-1197
2	US ARMY RSRCH LAB ATTN RDRL VTU V C KRONINGER ATTN RDRL VTU V A HARRINGTON ABERDEEN PROVING GROUND MD 21005
9	US ARMY RSRCH LAB ATTN RDRL CII A J TWIGG ATTN RDRL CIN B SADLER ATTN RDRL SER L A WICKENDEN ATTN RDRL SER L B PIEKARSKI ATTN RDRL SER L J PULSKAMP ATTN RDRL SER L R POLCAWICH ATTN RDRL SER L W NOTHWANG ATTN RDRL SER L G SMITH ATTN RDRL SER L J CONROY ADELPHI MD 20783-1197
1	CALIFORNIA INSTITUTE OF TECHNOLOGY ATTN MC 305-16 E WOLFF 1200 E CALIFORNIA BLVD PASADENA CA 91125
1	UNIVERSITY OF MARYLAND ATTN DANIEL SILVERSMITH 6801 PREINKERT DR., UNIT 7312B COLLEGE PARK MD 20742

NO. OF COPIES	ORAGANIZATION
1	UNIVERSITY OF PENNSYLVANIA MULTIMEDIA AND NETWORKING LABORATORY ATTN A KOPPEL 306 MOORE 200 SOUTH 33RD STREET PHILADELPHIA, PA 19104
1	UNIVERSITY OF CALIFORNIA BERKELEY ATTN DAN CALDERONE 337 CORY HALL BERKELEY, CA 94720-1772
1	HARVARD UNIVERSITY ATTN NICHOLAS PERKONS, 509 KIRKLAND M.C. 95 DUNSTER ST. CAMBRIDGE, MA 21038
1	CEDARVILLE UNIVERSITY ATTN MICHAEL COMPARETTO 251 N. MAIN STREET # 2554, CEDARVILLE, OH 45314
1	PRINCETON UNIVERSITY ATTN: YUAN CHEN 1471 FRIST CAMPUS CENTER PRINCETON, NJ 08544
1	VISHNU GANESAN 2280 SOUTH OVERLOOK ROAD, CLEVELAND OH, 44106
1	KESSHI JORDAN 14526 MACCLINTOCK DR. GLENWOOD, MD 21738
1	KATHRYN SCHNEIDER 8204 BALTIMORE AVE APT#1026C COLLEGE PARK, MD 20740
1	MICHAEL ROBERTS 12608 IVYSTONE LANE LAUREL, MD 20708
1	CORDELL REID 8531A GREENBELT RD, APT 202, GREENBELT MD 20770

NO. OF COPIES	ORAGANIZATION
1	TRISTAN HELMS 928 S STATE ST APT 4 ANN ARBOR, MI 48104
1	NAVAL SURFACE WARFARE CENTER ATTN JESSE CAMPBELL, K74 5370 MARBLE ROAD, SUITE 143 DAHLGREN, VA 22448-5165

TOTAL: 28 (1 ELEC, 27 HCS)

INTENTIONALLY LEFT BLANK.